JOURNAL OF GEOPHYSICAL RESEARCH, VOL. 105, NO. A9, PAGES 21,129–21,142, SEPTEMBER 1, 2000

Cusp field-aligned currents and ion outflows

R. J. Strangeway,[1] C. T. Russell,[1] C. W. Carlson,[2] J. P. McFadden,[2] R. E. Ergun,[3]
M. Temerin,[2] D. M. Klumpar,[4] W. K. Peterson,[4] and T. E. Moore[5]

Abstract. On September 24 and 25, 1998, the Polar spacecraft observed intense outflows of terrestrial ions in association with the passage of an interplanetary shock and coronal mass ejection. The orbit of the Fast Auroral Snapshot (FAST) Explorer was in the noon-midnight meridian during this ion outflow event, and FAST passed through the dayside cusp region at ~4000 km altitude every 2.2 hours. FAST was therefore able to monitor the ion outflows subsequently observed by Polar. We show that while the outflows were more intense after the shock passage, the overall particle and field signatures within the cusp region were qualitatively similar both before and after the shock passage. FAST observations show that the cusp particle precipitation marks the lower-latitude leg of a pair of field-aligned currents and further, that both field-aligned current sheets appear to be on open field lines. Moreover, the polarity of the cusp currents is controlled by the polarity of the interplanetary magnetic field (IMF) y-component, such that the magnetic field perturbation associated with the pair of cusp currents is in the same direction as the IMF B_y. This is a consequence of the reconnection of cusp-region field lines at the magnetopause, with the flux transport resulting in electromagnetic energy being transmitted along field lines to the ionosphere as Poynting flux. We show that this Poynting flux can be as high as 120 mW m^{-2} (120 ergs cm^{-2} s^{-1}) at FAST altitudes (~500 mW m^{-2} at ionospheric altitudes), presumably because of the strong IMF B_y (~40 nT), and is the dominant energy input to the cusp-region ionosphere. Furthermore, we find that the peak ion outflow flux is correlated with the peak downward Poynting flux, although only a few passes through the cusp centered around the time of the shock passage were used to determine this correlation. The energy carried by Poynting flux is dissipated as heat within the ionosphere, through Joule dissipation. The heating will tend to increase the ionospheric scale height, allowing greater access of ionospheric ions to the altitudes where transverse ion heating via ELF waves can occur. Thus electromagnetic energy supplied by the transport of reconnected magnetic flux is the essential first step in a multistep process that enhances the outflow of ionospheric plasma in the dayside cusp.

1. Introduction

Recently, *Moore et al.* [1999] reported on intense ion outflows observed by the Polar spacecraft. These outflows of ionospheric ions were associated with a sudden compression of the magnetosphere following the passage of an interplanetary shock. The shock was driven by a coronal mass ejection (CME). Following the shock passage, the interplanetary magnetic field (IMF) was initially northward but with a strong positive y-component. Later the IMF turned southward, with subsequent substorm activity within the magnetosphere. However, while the magnetosphere was moderately active prior to the passage of the interplanetary shock, the ion outflows observed at Polar do not appear to be related to substorm-generated outflows. *Moore et al.* [1999] therefore proposed an alternative explanation, based on an analysis of Dynamics Explorer 1 data presented by *Pollock et al.* [1988], where the outflows were caused by dynamic pressure fluctuations in the solar wind.

It should be noted, however, that *Moore et al.* [1999] did not give any specific mechanism for generating ion outflows by dynamic pressure fluctuations. Their conclusion is based mainly on the observation that of the various solar wind parameters, the standard deviation of the solar wind dynamic pressure shows the largest correlation with oxygen outflow flux. Moore et al. specifically noted that the correlation of the oxygen outflow with IMF-dependent parameters was poor. They took this to indicate that reconnection at the dayside magnetopause was not an important controlling factor.

On the basis of observations by the Fast Auroral Snapshot (FAST) Explorer we will argue instead that reconnection near the magnetospheric cusp controls the ion outflows. In a completely closed idealized magnetosphere the cusp is defined by the singular field line that maps to the entire magnetopause. In general, however, the cusp is not a singular field line but corresponds to a region in which field lines map close to the magnetopause. *Crooker* [1979] has shown that some of these cusp-region field lines can participate in antiparallel merging for any orientation of the IMF. For strongly southward IMF, reconnection tends to occur in the subsolar region, but the reconnection site can move to higher latitudes and away from noon, depending on the IMF clock angle. Other components of the IMF, such as the y-component, can therefore contribute to reconnection near the

[1]Institute of Geophysics and Planetary Physics, University of California, Los Angeles.
[2]Space Sciences Laboratory, University of California, Berkeley.
[3]Laboratory for Atmospheric and Space Physics, University of Colorado, Boulder.
[4]Lockheed Martin Advanced Technology Center, Palo Alto, California.
[5]NASA Goddard Space Flight Center, Greenbelt, Maryland.

Paper number 2000JA900032.
0148-0227/00/2000JA900032$09.00

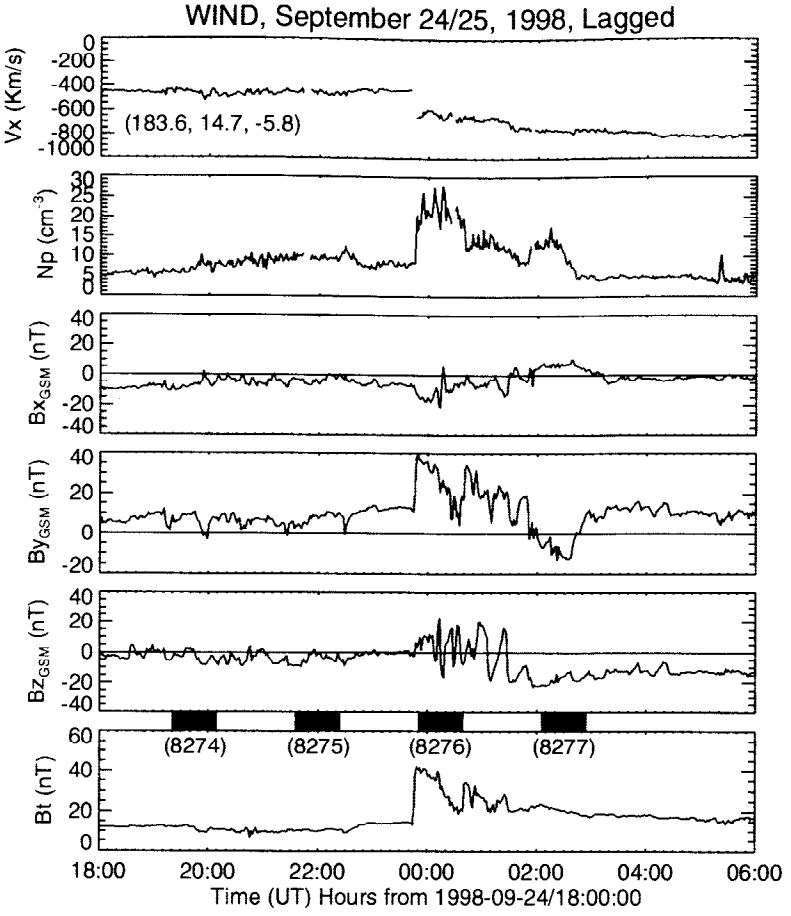

Figure 1. Solar wind data from the Wind spacecraft for the September 24-25, 1998, ion outflow event. The top panel shows the geocentric solar magnetospheric (GSM) x-component of the solar wind velocity. The next panel shows the solar wind density, while the bottom four panels show the interplanetary magnetic field (IMF) in GSM. The data have been lagged by 25 min, so that the interplanetary shock is coincident in time with the sudden impulse observed in the Earth's magnetosphere. The numbers in parentheses in the top panel give the Wind location in geocentric solar ecliptic (GSE) coordinates, in Earth radii. The bars above the total magnetic field indicate the times when the Fast Auroral Snapshot Explorer (FAST) spacecraft was in the northern auroral zone and polar cap, with the numbers in parentheses giving the corresponding orbit number.

cusp. To the extent that the reconnection site rotates about the cusp, we shall refer to this as cusp reconnection, but this includes the standard configurations for southward IMF (subsolar reconnection equatorward of the cusp) and northward IMF (reconnection tailward of the cusp). Since the rate of reconnection is likely to be enhanced following the passage of the interplanetary shock, we might expect field-aligned currents in the cusp region to be significantly larger after the shock passage. Larger cusp-region field-aligned currents will result in both larger ionospheric Joule dissipation and enhanced ELF/VLF emissions at low altitudes. These will in turn increase the ion outflow rates.

The outline of the paper is as follows. In the next section we will overview the FAST observations for the September 24-25 event. In section 3 we will discuss the observations in terms of the electromagnetic stresses applied to the ionosphere. We will also discuss different models of the cusp-region field-aligned current morphology. Section 4 will present more details of the relationship between electromagnetic energy input (Poynting flux) and the output ion fluxes. We will show a clear correlation for the albeit restricted set of data presented here. We will summarize our results and present conclusions in section 5.

2. September 24-25 Outflow Event: Overview

As noted in the introduction, the enhanced ion outflows reported by *Moore et al.* [1999] followed the passage of an interplanetary shock. The solar wind parameters for this interval, as observed by the Wind spacecraft, are shown in Figure 1. The data in this figure have been displaced to later times so that the time of the shock passage coincides with the time of the sudden impulse observed within the magnetosphere. The sudden impulse as observed by FAST is shown in Plate 1 and occurs at 2345 UT. The required lag time is ~25 min, which is consistent with the lag time expected for the observed solar wind velocity upstream of the interplanetary shock, given that Wind is ~180 R_E upstream of the Earth.

The top two panels of Figure 1 show the x-component of the solar wind velocity and the solar wind density. There is a significant enhancement of the solar wind dynamic pressure following the passage of the shock, ~15 nPa. *Moore et al.* [1999] suggest that it is the fluctuations in this dynamic pressure which cause the enhanced ion outflows observed by the Polar spacecraft. The bottom four panels of Figure 1 show the IMF, and we note that

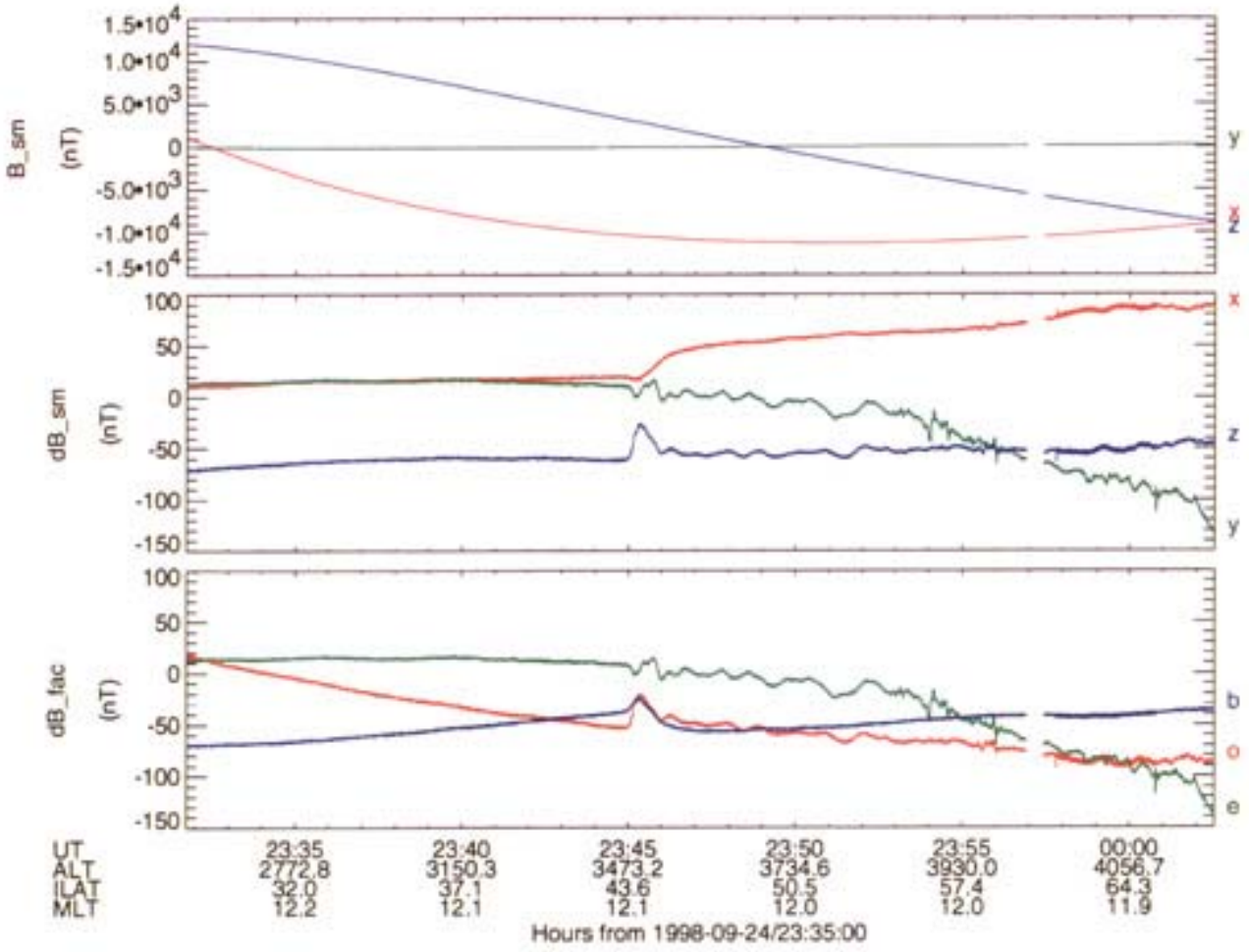

Plate 1. The September 24 sudden impulse as observed by FAST orbit 8276. The top panel shows the total magnetic field in solar magnetic (SM) coordinates, with the middle panel giving the deviations from the model field (IGRF 95 plus secular variation), also in SM. The bottom panel gives the deviations of the magnetic field in local field-aligned coordinates, as described in the text.

the IMF is also significantly enhanced following the shock passage, reaching a magnitude of 40 nT. Most of the field is in the y-GSM direction, with a weakly northward component. As noted in the introduction, reconnection with a y-directed IMF can occur near the cusp, and we will argue that this is the primary cause of the ion outflows observed on September 24-25.

Before presenting these arguments, we will summarize the FAST particle and field observations for this event. As previously noted, Plate 1 shows the sudden impulse as observed by FAST. The plate contains ~30 min of data, with the top panel showing the total magnetic field in solar magnetic (SM) coordinates, the middle panel showing the deviations from the model field (International Geomagnetic Reference Field (IGRF) 95 plus secular variation) in SM coordinates, and the bottom panel showing the deviations in local field-aligned coordinates. In this coordinate system curve b is parallel to the model field, and curve e is perpendicular to the plane defined by the model magnetic field and the radius vector to the spacecraft, with the positive direction pointing to the east. The third component, curve o, is outward, pointing toward more northerly latitudes in the Northern Hemisphere and toward more southerly latitudes for the Southern Hemisphere. The triad o-e-b forms a right-handed coordinate system.

At the time of the sudden impulse the ambient magnetic field is mainly in the x-SM direction, and the middle panel of Plate 1 shows that the sudden impulse is relatively smooth in this direction, while the field oscillates in the y and z directions. In field-aligned coordinates it is clear that these oscillations are mainly transverse, while the smoothly varying signal corresponds to a rarefaction of the field. The transverse oscillations are to be expected, although we cannot determine if these oscillations are due solely to "ringing" of the magnetosphere or if they correspond to oscillations driven externally by fluctuations in the solar wind. The rarefaction is less easily understood. An enhancement of the solar wind dynamic pressure would be expected to compress the magnetospheric field, resulting in fast-mode waves propagating throughout the magnetosphere. Perhaps the interplay of these various waves could give local rarefactions. For example, while there may be a compressional wave propagating from the dayside magnetopause, Polar shows that the lobe field strength also increases [*Russell et al.*, 1999]. The compressional wave which increases the sunward directed lobe field could reduce the tailward directed field on propagating to lower (FAST) altitudes. It appears that relatively sophisticated ray path calculations may be required to fully explain the signatures of the sudden impulse as a function of location within the magnetosphere.

Figure 1 provides the solar wind context for the changes which occur within the magnetosphere, while Plate 1 gives the timing of the sudden impulse driven by the interplanetary shock. Plate 2 presents an overview of the FAST particles and field observations. FAST is in an 83° inclination elliptical orbit with apogee near 4200 km. The orbit precesses ~3 hours in local time per month, and the orbit is near the noon-midnight meridian during the September 24-25 interval. Data from four passes of FAST through the northern auroral zone and polar cap are shown. Each panel is labeled by the corresponding orbit number. Two of the passes occur prior to the sudden impulse, and two occur after. The formats of the four panels are the same, showing ELF/VLF electric field spectra measured with the long (55 m) wire boom pair (Plate 2a); electron energy spectra averaged over all pitch angles (Plate 2b); electron pitch angle spectra averaged over energy from 5 eV to 30 keV (Plate 2c); ion energy spectra averaged over all pitch angles (Plate 2d); ion pitch angle spectra averaged over energy from 4 eV to 30 keV (Plate 2e); the spin-averaged perpendicular electric field in the spacecraft spin plane (Plate 2f); and the deviations of the magnetic field in SM coordinates (Plate 2g). The scales on the left-hand side of the plate apply to both columns, as do the color bars on the right. In particular, the field quantities in Plates 2f and 2g have the same scales in all four panels to facilitate intercomparison.

The ELF/VLF spectra are calculated on board the spacecraft, with the temporal resolution dependent on the spacecraft data rate. The data are not despun, and the resultant spin modulation (~2.5 s period) can be aliased to lower frequencies for low data rates. This is evident, for example, around 0010 UT on orbit 8276 for waves below 100 Hz. The white line in the spectra shows the local proton gyrofrequency.

The ion and electron electrostatic analyzers are designed to provide high-resolution energy and pitch angle data [*Carlson et al.*, 1998], with electrostatic deflectors being used to ensure that the ambient magnetic field falls within the 360° instantaneous field of view of the instrument. Again, the temporal resolution depends on the spacecraft data rate, with the shortest sampling interval being 70 ms.

The electric field component shown in Plate 2f, labeled "E along V_{sc}," is obtained by spin fits to the higher-resolution data. The spin fits provide a value of electric field every half spin (~2.5 s). The spacecraft spin axis is nearly perpendicular to the spacecraft orbit plane, and the $\mathbf{V}_{sc}\times\mathbf{B}$ electric field is therefore very small in the spin plane. Nevertheless, we have removed this small correction to the spin-plane electric field. Because the spacecraft velocity is close to the spin plane, this component of electric field is labeled "E along V_{sc}" for convenience. The name also emphasizes that there is no $\mathbf{V}_{sc}\times\mathbf{B}$ contribution to this electric field component.

The deviations of the magnetic field shown in Plate 2g are calculated with respect to the IGRF 95 model field, including secular variation. The model field, which is a spherical harmonic expansion to the ambient field, does not include any fields caused by sources external to the Earth. Thus perturbations due to the ring current, magnetopause currents, the tail current, or field-aligned currents are not included. This may be important when we later discuss the forces applied to the ionosphere.

In Plate 2, about 40 min of data are shown for each orbit. For these orbits the spacecraft trajectory is near the noon-midnight meridian, with apogee near 70° invariant latitude on the dayside. The four orbits are similar, with the spacecraft initially on closed field lines within the dayside magnetosphere, as evidenced by the double loss cone in the ion distributions. At the same time, high-energy trapped electrons are also observed, as well as lower-energy electrons in the source cone. These low-energy electrons are photoelectrons escaping from the atmosphere. As the spacecraft moves to higher latitude, the ions often show a single loss cone. While a double loss cone is a clear indication of closed field lines, the presence of a single loss cone is not an unambiguous indicator of open field lines because pitch angle scattering near the magnetic equator could fill the loss cone. Similarly, the absence of a source cone distribution of downgoing photoelectrons is not unique to open field lines. The clearest indicaton of the passage of the spacecraft onto open field lines is the disappearance of >1-keV trapped electrons. These three signatures are particularly clear for orbit 8275, where for increasing latitude the spacecraft observes the single loss cone in the ions, the single source cone in the electrons, and the disappearance of >1-keV electrons.

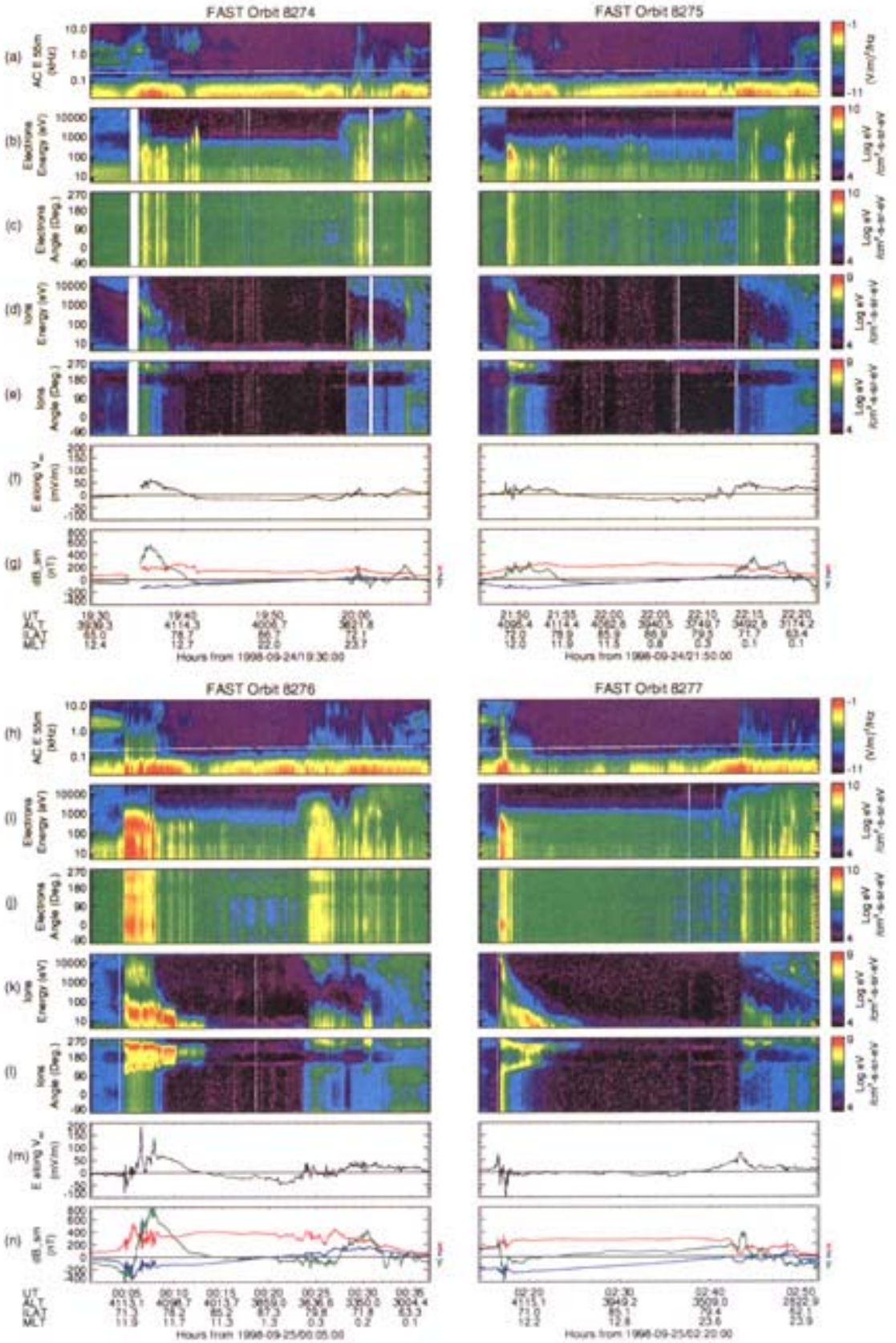

Plate 2. Overview plots of FAST data for the September 24-25 ion outflow event. Two orbits before the sudden impulse (8274 and 8275) and two orbits after (8276 and 8277) are shown. The different data quantities are described in more detail in the text.

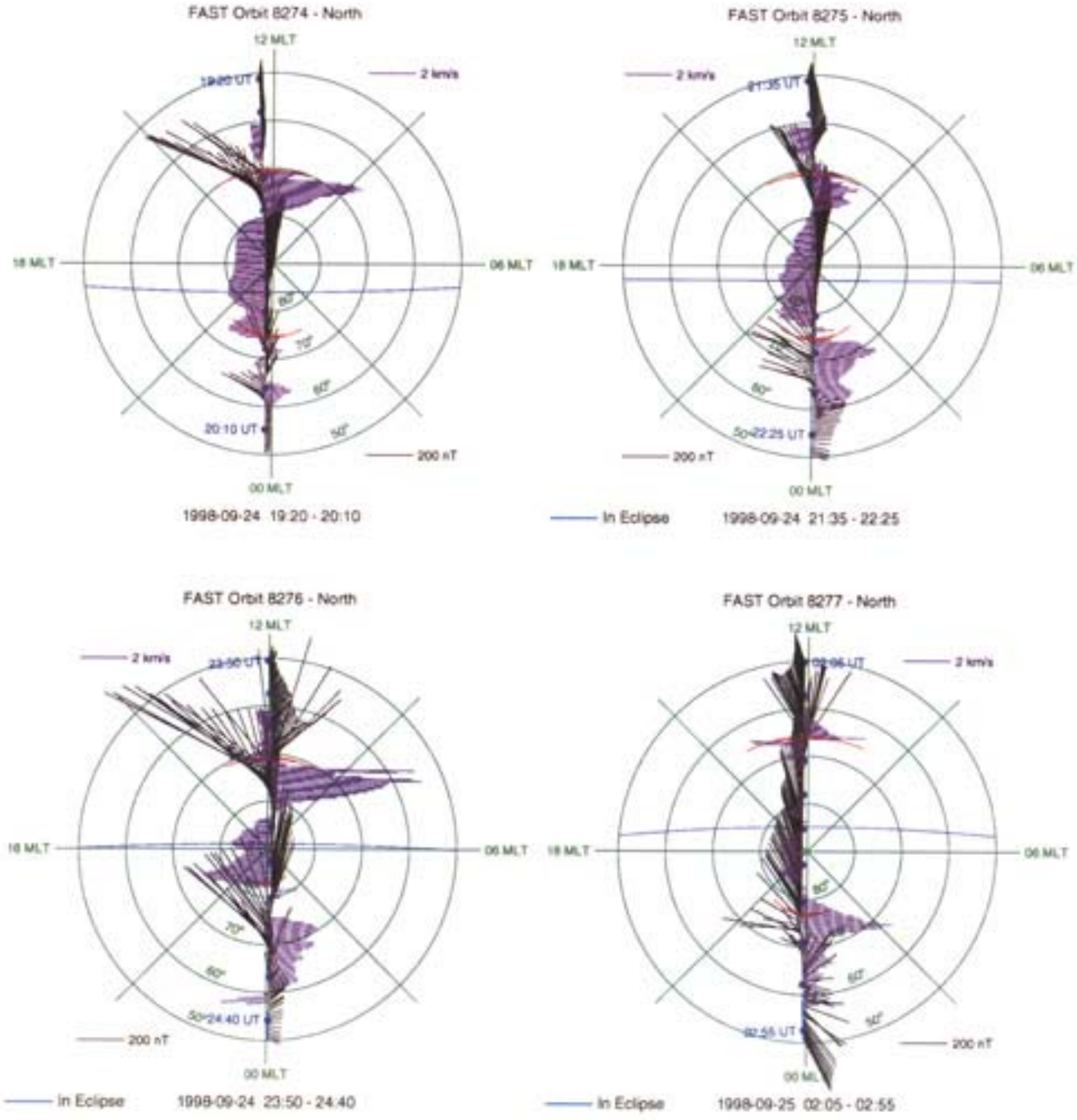

Plate 3. Polar projections of the perturbation magnetic field and equivalent flow velocity for the orbits shown in Plate 2. The red arc segments mark the polar cap boundary, as discussed in the text.

Cusp precipitation, which is characterized by an enhancement in ~keV ions that show a decrease in energy for increasing latitude, is observed as the spacecraft passes onto open field lines. Lower-energy ions are also observed, often as ion conics. Data from the time-of-flight energy angle mass spectrograph on FAST [*Carlson et al.*, 1998] (not shown) indicate that the ~keV ions are primarily protons, while the ion conics are O^+. A strong deflection in the y-SM component of the magnetic field is also observed in conjunction with the cusp ions. On comparison with the data in Figure 1, it is apparent that for each pass the deflection in the magnetic field is in the same direction as the y-GSM component of the IMF. This signature is that expected for reconnection of cusp field lines [*Cowley*, 1981].

At higher latitudes the slope of the magnetic field perturbation changes sign. It appears that the region of cusp precipitation marks one polarity of field-aligned current, with the opposite polarity (return) current extending to higher latitudes in the polar cap. The return current region tends to be more extended in latitude. With a meridional pass, however, we cannot address the longitudinal extent of the current-carrying regions, nor can we address the issue of longitudinal versus latitudinal current closure within the ionosphere.

The electric field in Plate 2 often tracks the deviation in the y-component of the magnetic field, at least in the cusp region. These two components are close to perpendicular to each other, and their cross product corresponds to Poynting flux. The Poynting flux is downward when the y-SM component of the magnetic field and the "E along V_{sc}" component of the electric field have the same sign.

At higher latitudes, including the return current region, the spacecraft is clearly in the polar cap. For the first three orbits, sporadic bursts of few 100-eV electrons are observed. These may be magnetosheath or mantle electrons, although the IMF is mainly northward. *Bonnell et al.* [1999] have discussed the possible sources of precipitating electrons within the polar cap for northward IMF. Sources include the magnetosheath, the low-latitude boundary layer, and the nightside plasma sheet. They argued in favor of a magnetosheath origin for specific field-aligned current related signatures, but it is not clear if the same arguments apply for all precipitating electron signatures. In contrast, polar rain extends across most of the polar cap for orbit 8277, when the IMF is southward, suggesting that the magnetosheath electrons have access to almost the entire polar cap.

The spacecraft passes into the nightside auroral oval toward the end of each pass. Since our main purpose here is to emphasize the cusp-region observations, we will not discuss the auroral zone signatures in detail, except to note that the polar cap is very small for orbit 8276. The spacecraft leaves the polar cap at ~83° invariant latitude on this orbit.

The overall impression given by Plate 2 is that the FAST observations are qualitatively similar for each orbit. The spacecraft first passes from a region of closed to open field lines. It then encounters a region of cusp precipitation and an associated field-aligned current whose polarity depends on the y-component of the IMF. The cusp also includes a region of outflowing ion conics. A lower-density return current is found at higher latitudes. The spacecraft then continues across the polar cap, exiting through the near-midnight auroral zone.

The most obvious signature of the post sudden impulse orbit (8276) is the increase in the magnitude of the particle fluxes and in the magnetic and electric field strengths. We will argue in the next section that the enhanced fields are caused by increased reconnection of cusp-region magnetic fields. The associated Poynting flux carries energy into the ionosphere. The resultant Joule dissipation, together with ion heating by field-aligned current driven instabilities, is the probable cause of the ion outflows.

3. Magnetosphere-Ionosphere Coupling

Having presented an overview of the FAST particles and fields data during the September 24-25 ion outflows, we will now address the source of these outflows. Our basic thesis is that the ion outflows are a consequence of the enhanced Joule dissipation in the cusp-region ionosphere. The ionospheric Joule dissipation involves Pedersen currents, and these currents are driven by field-aligned currents, which in turn are driven by perpendicular currents in the high-altitude magnetosphere.

The framework within which we view the current systems has been referred to as the "B, v paradigm" [*Parker*, 1996]. Figure 2 [from *Strangeway et al.*, 2000] shows a sketch of how transport of reconnected field lines at the magnetopause can drive currents in the ionosphere. We assume that there is a region of enhanced flux transport at the magnetopause. This transport produces a shear in the flow velocity and the magnetic field. The magnetic field shear corresponds to a field-aligned current. At the magnetopause the perpendicular current which closes the field-aligned currents opposes the motional electric field, and the magnetopause is a generator for electromagnetic energy. The field-aligned currents close in the ionosphere as a Pedersen current. This current provides a $\mathbf{j}\times\mathbf{B}$ force, which is required to move the ionospheric plasma against the frictional force caused by collisions between ions and the neutral atmosphere. In terms of magnetic stresses, the ionospheric drag results in increased field line tension. The perturbation field ($\delta\mathbf{B}$), which is out of the plane of Figure 2, together with the $\mathbf{V}\times\mathbf{B}$ electric field, corresponds to a Poynting flux ($\mathbf{E}\times\delta\mathbf{B}/\mu_0$) from the magnetopause to the ionosphere. At the ionosphere this energy is dissipated through Joule

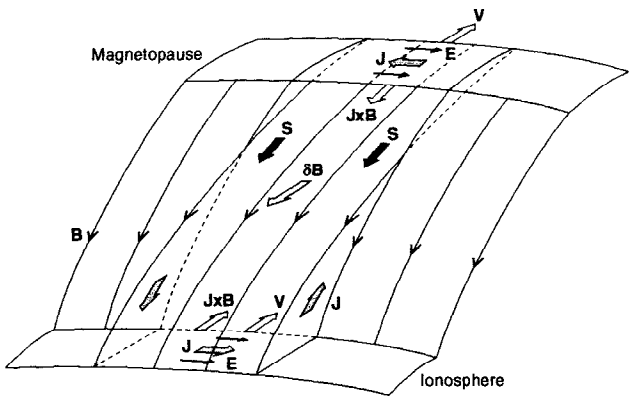

Figure 2. Schematic of the electrodynamic coupling between the magnetopause and the ionosphere [*Strangeway et al.*, 2000]. The magnetopause transport of reconnected flux tubes with velocity **V** "pulls" the field lines at the ionosphere, where the plasma motion must overcome the frictional drag. The $\delta\mathbf{B}$ associated with field-line stretching also implies perpendicular currents (**J**), which provide the necessary $\mathbf{J}\times\mathbf{B}$ force. These currents close through field-aligned currents. The motional electric field (**E**) opposes the current at the magnetopause, which is a generator of electromagnetic energy. This energy is dissipated in the ionosphere where $\mathbf{J}\cdot\mathbf{E} > 0$. The electromagnetic energy is transmitted through Poynting flux ($\mathbf{S} = \mathbf{E}\times\delta\mathbf{B}/\mu_0$).

dissipation. The amount of Joule dissipation depends on both the driving forces and the amount of ionospheric drag, which is closely related to the Pedersen conductivity.

Following *Strangeway et al.* [2000], we can derive some scaling laws which relate the FAST observations to higher-altitude fields and flows. Mapping of the convection electric field gives

$$V_I B_0 L_I = f V_m B_n L_m, \tag{1}$$

where V_I is the ionospheric plasma flow velocity with respect to the neutral atmosphere, B_0 is the ambient ionospheric magnetic field, L_I is the transverse scale length (in the direction of the horizontal current) at the ionosphere, V_m is the flow velocity at the magnetopause, B_n is the normal component of the magnetic field through the magnetopause, and L_m is the transverse scale at the magnetopause. The parameter f is related to the degree to which field lines are equipotentials. When $f = 1$, the electric field mapping is perfect (no parallel electric fields). When $f = 0$, the shielding is perfect (no ionospheric electric fields).

From current continuity,

$$J_I/B_0 L_I = J_m/B_n L_m, \tag{2}$$

where J_I is the ionospheric current intensity and J_m is the magnetopause current intensity.

From Ampere's law the magnetic field perturbation for a current sheet of intensity $J = \delta B/\mu_0$, and (2) can be rewritten as

$$\delta B_I/B_0 L_I = \delta B_m/B_n L_m. \tag{3}$$

Last, at the ionosphere,

$$J_I = \Sigma_P V_I B_0 \tag{4}$$

where Σ_P is the height-integrated Pedersen conductivity.

Rearranging (4) and replacing the current intensity by the magnetic field perturbation,

$$V_I = -\frac{\delta B_I}{\mu_0 \Sigma_P B_0}. \tag{5}$$

The minus sign in (5) gives a vector relationship, even though the equation is written in terms of scalar quantities. The minus sign arises because the ambient magnetic field is downward in the Northern Hemisphere and the velocity and the magnetic field perturbation are in opposite directions. For the Southern Hemisphere the flow velocities and magnetic field perturbations would be in the same direction.

These equations can be used to relate the fields and flows at the magnetopause to ionospheric observations. From (3) and (4),

$$\delta B_m = -\mu_0 \Sigma_P \frac{L_m}{L_I} V_I B_n, \tag{6}$$

while from (1) and (5),

$$V_m = -\frac{1}{f \mu_0 \Sigma_P} \frac{L_I}{L_m} \frac{\delta B_I}{B_n}. \tag{7}$$

Again, the minus sign applies for the Northern Hemisphere. Equations (6) and (7) include the length scale ratio, L_m/L_I. This ratio approximately equals $(B_0/B_n)^{1/2}$.

Equations (6) and (7) can be combined to give

$$f V_m \delta B_m = V_I \delta B_I. \tag{8}$$

Since $V_m = E_m/B_n$ and $V_I = E_I/B_0$, where E_m and E_I are magnetospheric and ionospheric electric fields, respectively, (8) states that the Poynting flux into the ionosphere equals that fraction of the Poynting flux from the magnetopause or magnetosphere that is not lost through Joule dissipation along the magnetic field lines.

To demonstrate the appropriateness of these scaling laws, we will use the cusp region observations from orbit 8274 in Plate 2. Although the scaling laws use ionospheric parameters, we can use local FAST observations since all the quantities scale as $(B_0/B)^{1/2}$, or its inverse, where B is the local magnetic field strength. Dropping the subscript for quantities at FAST altitudes, near 1937 UT $E \approx 60$ mV m^{-1}, while $\delta B \approx 600$ nT. From (5), $\Sigma_P \approx 8$ S, which is reasonable for the dayside ionosphere. At FAST, $B \approx 13{,}000$ nT and the flow velocity $V \approx 4.6$ km s^{-1} for $E \approx 60$ mV m^{-1}. From (6), assuming $B_n \approx 5$ nT, $\delta B_m \approx 12$ nT, while from (7) $V_m \approx 230$ km s^{-1}. These numbers are not unreasonable for the fields and flows at the magnetopause.

To more easily visualize the forces and flows observed by FAST, we have converted the magnetic and electric field data shown in Plate 2 to a polar projection in Plate 3. The black vectors give 20-s averages of the transverse magnetic field perturbations, plotted as a function of magnetic local time and invariant latitude along the spacecraft trajectory. The purple vectors give 20-s averages of the "E along V_{sc}" electric field, converted to an equivalent flow velocity. The magnetic field perturbations include both along-track and perpendicular components, but the flow velocity is only determined for the direction nearly perpendicular to the spacecraft trajectory. In the spirit of the previous discussion, the black vectors give the forces imposed on the ionosphere, while the purple vectors give the resultant flows. The blue dots along the spacecraft trajectory give 5-min tick marks, while the blue line marks the terminator at the foot of the field line.

The red arc segments mark the polar cap boundary inferred from the disappearance of >1-keV electrons. Plate 3 shows that the polar cap boundary on the dayside is often near a flow velocity reversal. The magnetic field deflection, which closely tracks the flow velocity, suggests that the cusp-region field-aligned currents are mainly on open field lines. Recently, *Amm et al.* [1999] have reported a similar conclusion, although their results were for IMF $B_z < 0$. These authors argue that their observations support a model put forward by *Lee et al.* [1985], in which the cusp-region field-aligned currents are ultimately related to magnetopause currents. Lee at al. refer to "current leakage" of magnetopause currents as the cause of cusp-region field-aligned currents and contrast their model to *Cowley* [1981], among others. In particular, Lee et al. suggest that Cowley considered enhanced ionospheric flows in the dayside "throat" to be the source of the field-aligned currents, because closure of the ionospheric currents associated with such flows will require field-aligned currents. In our opinion, this is perhaps a misreading of Cowley, and the two models are in fact similar, in that in both models the flows are ultimately driven by reconnection. As Figure 2 suggests, field-aligned currents are a natural consequence of such flows, since the closure of these currents within the ionosphere provides the $\mathbf{j}\times\mathbf{B}$ force to move the ionosphere. Indeed, we would argue that without the ionosphere there is no need for field-aligned currents. In this regard, the field-aligned currents are not simply "leakage" currents but an integral part of the coupling between the magnetopause and the ionosphere.

Figure 3, after *Cowley* [1981], shows the expected convection pattern within the polar ionosphere for a positive IMF B_y. The magnetic field perturbation is opposite to the plasma flow in the Northern Hemisphere, and there is remarkable qualitative agreement between Figure 3 and the data in Plate 3. The region of strong flows near noon in the sketch is the throat mentioned above, and the magnetic field perturbations are largest in the throat region, with weaker oppositely directed flows at higher latitudes corresponding to the convection cell centered on the duskside. For orbit 8277 these signatures are reversed, as

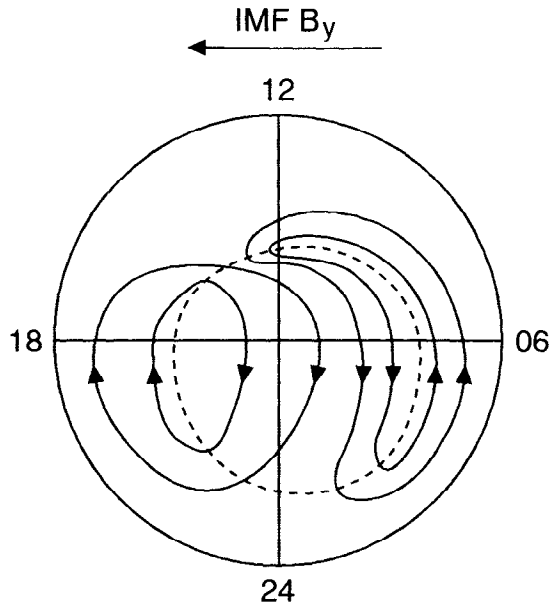

Figure 3. Schematic of the expected polar cap flows associated with a positive IMF B_y, after *Cowley* [1981].

expected given the change in sign of the IMF B_y. Furthermore, the polar cap flows are dominated by the antisunward convection expected for southward IMF.

Orbit 8277 is also interesting in another way, as this orbit demonstrates some of the difficulties inherent in determining the Poynting flux, that is, the direction in which electromagnetic energy flows. If we assume that the magnetic field $\mathbf{B} = \mathbf{B}_0 + \delta\mathbf{B}$, where $\mathbf{B}_0$ is the background field and $\delta\mathbf{B}$ is a perturbation field, and further that $\nabla\times\mathbf{B}_0 = 0$ everywhere (as is the case for the IGRF model field), then the Poynting flux is given by

$$\mathbf{S} = \mathbf{E}\times\delta\mathbf{B}/\mu_0 = (\mathbf{V}(\delta\mathbf{B}\cdot\mathbf{B}_0) - \mathbf{B}_0(\mathbf{V}\cdot\delta\mathbf{B}))/\mu_0, \quad (9)$$

where we have assumed $\mathbf{E} = -\mathbf{V}\times\mathbf{B}_0$.

The first term on the right-hand side of (9) corresponds to transport of magnetic flux. In the absence of field-aligned flows, only the last term corresponds to Poynting flux along the ambient magnetic field. In the cusp region the flow velocity is oppositely directed to the magnetic field perturbation, at least in terms of the across-track components, and the Poynting flux is downward. As Figure 2 indicates, this is to be expected when stress is applied at high altitudes. For orbit 8277, however, although most of the perturbation magnetic field is sunward in the polar cap, the across-track perturbation field and flow velocity are parallel. Thus the contribution to the Poynting flux from this component is apparently upward. (We do not know the amount of Poynting flux associated with the along-track component.) On the other hand, the phase relation between the electric field and the magnetic field suggests that the Poynting flux may be downward. In particular, just after 0228 UT both the electric field and the y-SM component of the magnetic field in Plate 2 show a positive displacement. For the electric field this results in a movement toward zero, while for the magnetic field the effect is a movement toward larger positive values. If we take only the direction of the displacement, then the two displacements are in phase, and the Poynting flux is apparently downward.

This contradiction is indicative of potential errors in the subtraction of the model field, which is required to determine the magnetic field perturbation, and is related to the fact that the Poynting flux as defined by (9) can, in principle, be split into two terms, $\mathbf{S} = \mathbf{S}_c + \mathbf{S}_d$, where we assume $\nabla\cdot\mathbf{S}_c = 0$ over the volume of interest, in this case the polar ionosphere. (The subscript c indicates that within the volume $\mathbf{S}_c$ is carried by curl-free magnetic fields, while the subscript d indicates that within the volume $\nabla\cdot\mathbf{S}_d \neq 0$.) $\mathbf{S}_c$ therefore does not contribute to $\nabla\cdot\mathbf{S}$. Ideally, we should further separate the perturbation field into two parts, $\delta\mathbf{B} = \mathbf{B}_0' + \delta\mathbf{B}'$ with $\nabla\times\mathbf{B}_0' = 0$ inside the volume of interest. Thus the ideal model field would be $\mathbf{B}_0 + \mathbf{B}_0'$. Uncertainties in the Poynting flux can therefore be attributed to two effects. The first is having a model field for which $\nabla\times\mathbf{B} \neq 0$ within the volume of interest. The second is including within the perturbation field $\delta\mathbf{B}$ fields for which $\nabla\times\mathbf{B} = 0$ within the volume of interest. Errors in spacecraft attitude and the model field both contribute to uncertainties of the second kind.

The model field used here only includes the IGRF field ($\mathbf{B}_0$), and $\nabla\times\mathbf{B}_0 = 0$ everywhere for this model field, ensuring that the only uncertainties in the Poynting flux are of the second kind. We have not estimated the additional model field $\mathbf{B}_0'$ due to external current systems. Unfortunately, including external fields in the model can also introduce problems, especially models such as the *Tsyganenko* [1996] (T96) model or other models which include current systems that close in the ionosphere, as this would introduce an uncertainty of the first kind discussed above. This statement is not a criticism of such models, but rather a recognition that these models may include the very fields we wish to analyze. Also, for this orbit the T96 model gives very little correction to the y-SM component because the spacecraft is near the noon-midnight meridian. This correction is even smaller if the region 1 and 2 current systems are turned off in the model. Second, small errors in the attitude of the spacecraft may be important. For example, an error of 0.1° in a 15,000-nT field will give an error of ~25 nT. The uncertainty in the spacecraft attitude is of this order.

As a mitigating factor, we should also point out that the Poynting flux carried by the fields in the polar cap for orbit 8277 is ~1 mW m^{-2}, whereas the Poynting flux in the cusp region is of the order of tens of milliwatts per square meter. If we take 1 mW m^{-2} as an estimate of the potential error in our Poynting flux calculation, then the direction and magnitude of the cusp-region Poynting flux are well determined.

As a last comment on the cusp-region magnetic field observations before discussing their relationship to the ion outflows, we have been intentionally imprecise in labeling the cusp-region currents. Several authors have assigned different names to these currents. For example, *Lee et al.* [1985] consider the lower-latitude current to be an extension of the region 1 current, while they refer to the higher-latitude current as the cusp current. The FAST data indicate that cusp precipitation is observed in conjunction with the lower-latitude current. Thus referring to the higher-latitude current as the cusp current may cause confusion, since that current is not associated with cusp precipitation. In contrast, *Wilhjelm et al.* [1978] suggest that the cusp-region field-aligned currents associated with the ionospheric *DPY* current system are independent of the region 1 currents.

To clarify the differences in the different models, we sketch three different configurations in Figure 4. Figure 4a is closest to the *Wilhjelm et al.* [1978] picture. The polarity of the two isolated field-aligned currents changes sign for the opposite polarity of the IMF. Figure 4b is similar to that proposed by *Lee et al.* [1985], while Figure 4c corresponds most closely to the convection pattern of *Cowley* [1981]. The data in Plate 3 seem to be most consistent with Figure 4c, but it should be noted that this

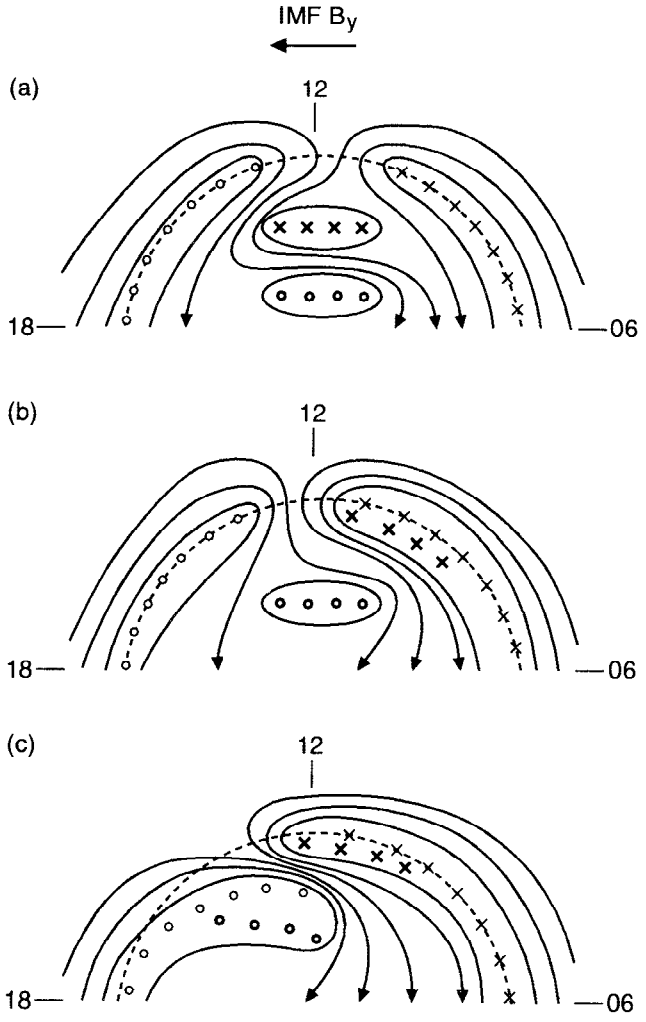

Figure 4. Sketches of the different possible cusp-region field-aligned current configurations and the associated polar cap convection. Only the dayside part of the polar cap is shown, and only the region 1 and cusp currents. The configurations shown are based on (a) the cusp-region currents invoked to explain the *DPY* current [*Wilhjelm et al.*, 1978], (b) the model of *Lee et al.* [1985], and (c) as implied by the convection pattern of *Cowley* [1981]. Apart from Figure 4c, we assume that the region 1 currents lie on the polar cap boundary, indicated by the dashed line. The flows for the opposite polarity of IMF B_y are obtained by mirror reflection about the noon-midnight meridian. The current configuration is also obtained by mirror reflection, but the polarity of the currents must be reversed. Currents into the ionosphere are indicated by crosses, while outward currents are indicated by circles, with bold symbols marking the cusp-region currents. For simplicity we have only sketched ionospheric flows from closed to open field lines, but for sufficiently weak region 1 currents the flows associated with the cusp currents in Figure 4a could be entirely within the polar cap, corresponding to circulation on open field lines.

may be because the IMF B_y is very large. In addition, the FAST trajectory is in the noon-midnight meridian for the storm interval under investigation, and we cannot bring any FAST data to bear on the east-west extent of the current sheets. One possible resolution is that the sketches in Figure 4 show a progression from strongly northward IMF, in Figure 4a, to strongly horizontal IMF, in Figure 4c. In particular, the orientation of the cusp-current system in Figure 4a could rotate depending on the IMF orientation, becoming the *NBZ* current system [*Zanetti et al.*, 1984] for mainly northward IMF. For the *NBZ* currents the downward current is in the afternoon sector and the upward current is in the morning sector. For positive IMF B_y the *NBZ* current system might be expected to rotate clockwise, tending toward the configuration shown in Figure 4a. For negative IMF B_y the rotation would be anticlockwise. Furthermore, although Figure 4a only shows convection from closed to open field lines, the cusp-region currents could result in entirely polar cap convection for sufficiently weak region 1 currents, i.e., circulation on open field lines. For purely northward IMF this would correspond to the four-cell convection pattern associated with the *NBZ* current system [*Zanetti et al.*, 1984]. As the northward IMF weakens, the cusp currents could begin to merge with the region 1 currents, as implied by Figures 4b and 4c, and convection from closed to open field lines would dominate.

4. Relationship Between Ion Outflows and Cusp-Region Poynting Flux

In the previous section we emphasized the electromagnetic coupling between the magnetosphere and the ionosphere. We specifically discussed the cusp-region field-aligned currents, which are associated with reconnection. The cusp currents appear to exist for all orientations of the IMF, indicating that some form of reconnection is always occurring near the cusp. These cusp currents may merge with the region 1 currents, especially for southward IMF. We also emphasized that the transport of magnetic flux at the magnetopause results in Poynting flux into the ionosphere.

We will now discuss the FAST observations for the most intense ion outflows, which occurred on orbit 8276, after the sudden impulse. Plate 4 is an expanded view of the cusp region on orbit 8276. Plates 4a-4c show electron spectra, with Plates 4b and 4c showing pitch angle spectra for electron energies greater and less than 100 eV, respectively. The higher-energy electrons appear to be mainly of magnetosheath origin, showing isotropic spectra, apart from the well-defined loss-cone. The lower energy electrons are bidirectional, indicating the presence of strong wave-particle interactions.

Plates 4d-4f show ion data. The energy spectra in Plate 4d show step-like features for the higher energies. *Lockwood and Smith* [1994] have suggested that this is a feature of pulsed reconnection. The pitch angle spectra for ions >300 eV, shown in Plate 4e, are also indicative of magnetosheath plasma entry. Ion composition data show that these ions are mainly protons. The lower-energy ions, in Plate 4f, are primarily oxygen and are clearly ion conics. These conics constitute the ion outflow.

Plate 4g shows the magnetic field deviations, and there is a strong downward current from ~0005 to ~0008 UT. This current is clearly collocated with the cusp precipitation. The magnetic field also shows a large degree of small-scale structure. Cartoons such as those presented in the previous section cannot easily explain such structure, which could be both temporal and spatial in origin.

Figure 5 shows the upward ion number flux and downward Poynting flux, as measured at FAST altitudes. The y-SM component of the magnetic field deviations is also shown. There is a clear overall correlation between the ion flux and the Poynting flux, although there is less of a correlation at the detailed level. In particular, the two sharp peaks in Poynting flux appear to be associated with reductions in the ion flux. Plate 4 shows a signifi-

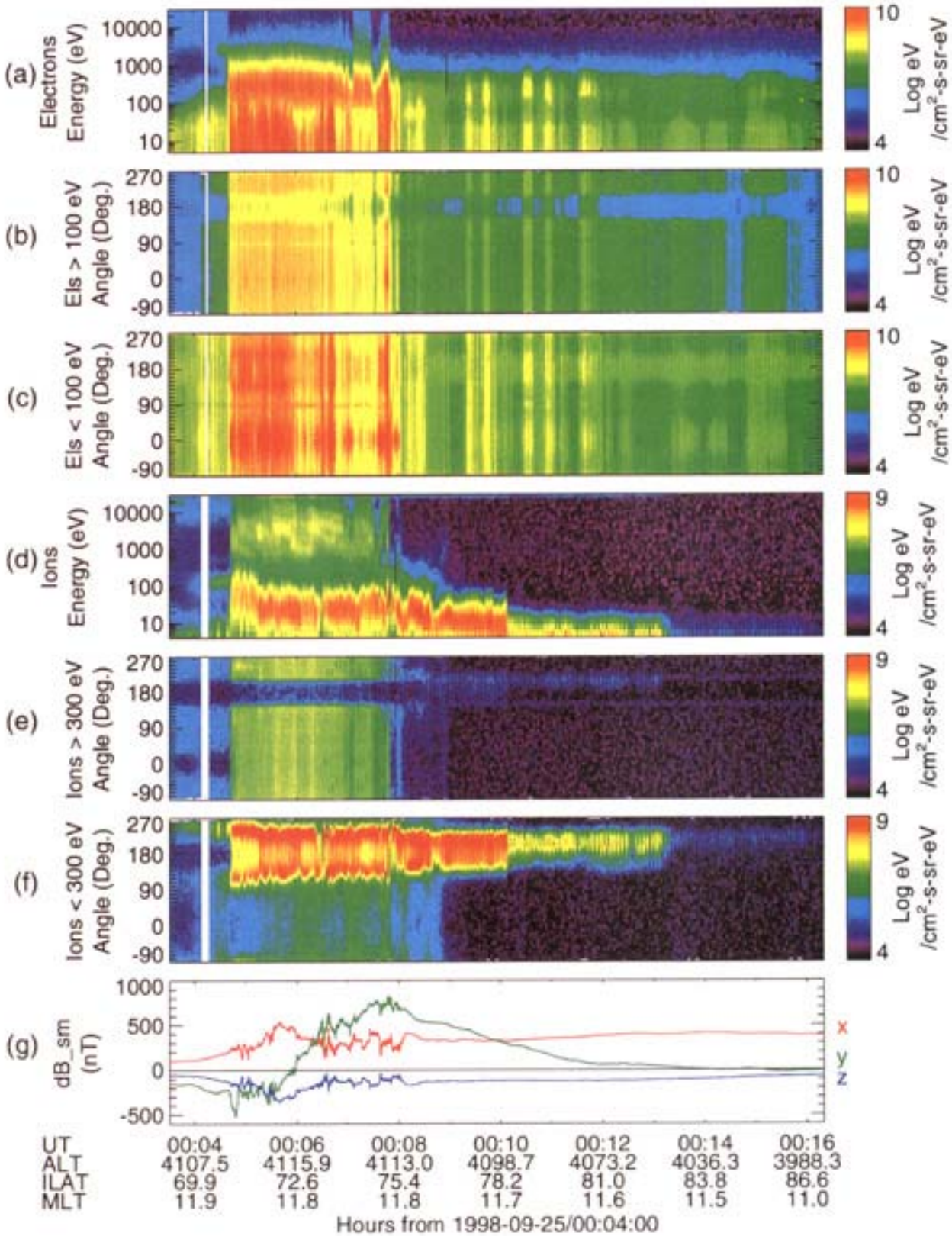

Plate 4. Expanded view of the cusp-region particle data for FAST orbit 8276. Plates 4a-4c show electron data, Plates 4d-4f show ion data, and Plate 4g shows the magnetic field deviations. The particle pitch angle spectra are displayed for both high and low energies, with the higher energies consisting mainly of magnetosheath and perhaps boundary layer plasma.

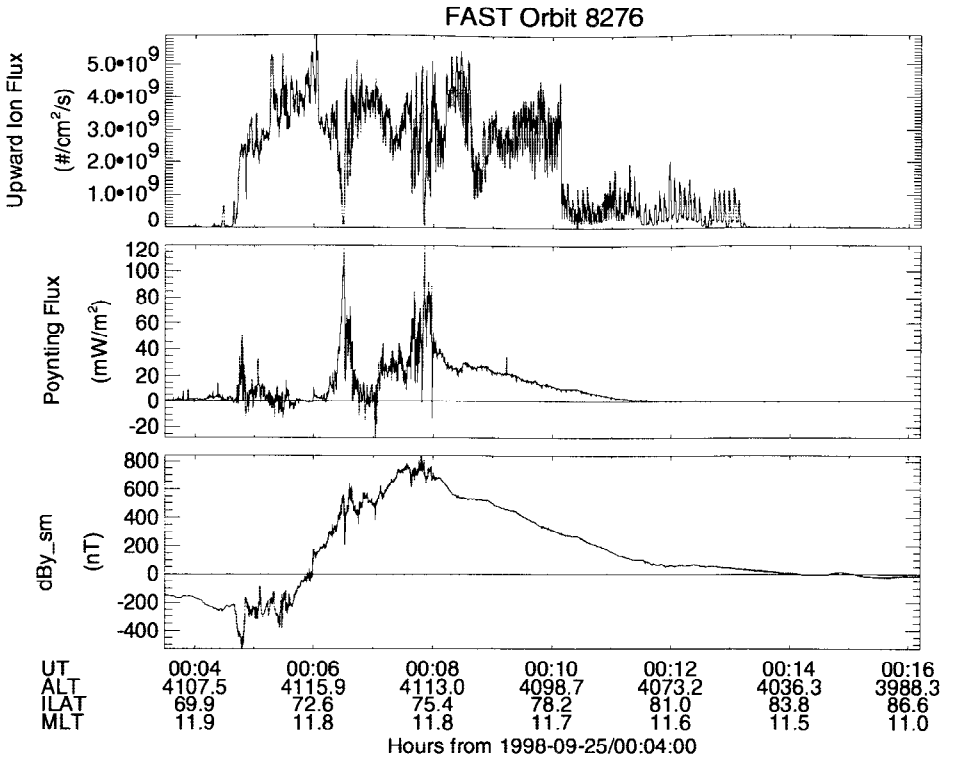

Figure 5. Upward ion flux and downward Poynting flux during the orbit 8276 cusp crossing. For reference we also include the y-SM component of the magnetic field deviations.

cant amount of structure in the magnetic field, indicative of smaller-scale field-aligned currents. These field-aligned currents are in addition associated with increased fluxes of <100-eV electrons, an indication that parallel electric fields are also present. Thus while the Poynting flux is the dominant energy input into the ionosphere (compare with the electron energy flux, ~ 5mW m^{-2} at this time), other factors, such as parallel electric fields, will affect the ion outflow, and detailed agreement is not to be expected.

In investigating the possible source of ion outflows, *Moore et al.* [1999] used the peak ion flux as a measure of the outflows. We will use the same parameter here. The peak Poynting flux will be used to characterize the energy input. Figure 6 shows the variation of peak ion flux with peak Poynting flux. Each point in the figure corresponds to a single pass through the cusp region, and data from five passes are shown. We have included data from orbit 8278, in addition to the four orbits discussed earlier. There is a clear correlation between the peak ion flux and the peak Poynting flux, but it should be remembered that data from only five orbits have been used.

It is not entirely obvious that the two parameters chosen best characterize either the energy input or the ion output. For example, one might consider ion energy flux as a better measure. We find, however, that the correlation is weaker and that the energy conversion is relatively inefficient, in that only ~0.1% of the Poynting flux is converted to outflowing ion energy flux. We also find that other measures, such as integrated fluxes, are less well correlated. We conclude that the correlation shown in Figure 6 is strongly indicative of a causal relationship, but additional data should be analyzed.

The exact mechanism relating the energy input to the ion outflow has not been specified. Poynting flux corresponds to the input of electromagnetic energy, and the previous discussion shows how transport of reconnected field lines at the magnetopause is a source of electromagnetic energy. That reconnection is the dominant mechanism for providing Poynting flux is made

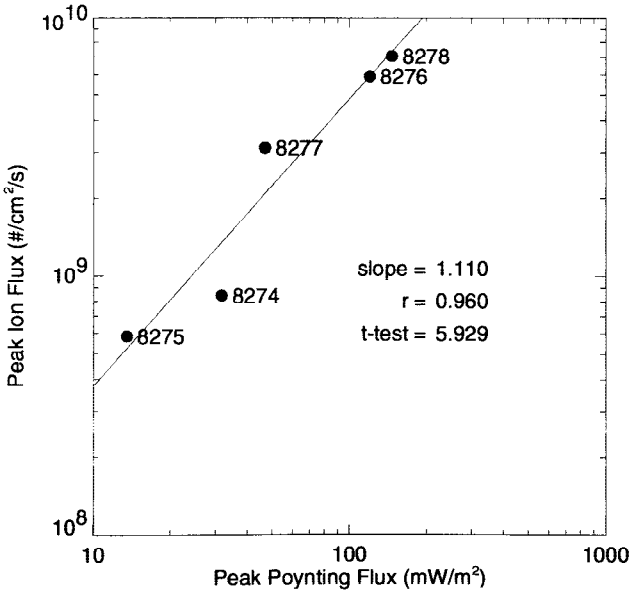

Figure 6. Peak ion flux as a function of peak Poynting flux. Peak fluxes are shown for five consecutive passes through the dayside cusp, with each point being labeled by its respective orbit number. Orbits 8274 and 8275 occurred before the sudden impulse. The two-tail 99% significance level for the student's t-distribution is 5.841.

clear by the observation that the cusp-region field-aligned current polarity is controlled by the IMF B_y. The Poynting flux will be converted to heat in the ionosphere through Joule dissipation. (That the Poynting flux is mainly dissipated as heat may explain the low conversion efficiency in terms of ion energy fluxes.) This dissipation is mediated by ion-neutral collisions. Besides heating the neutrals, some of the dissipation will convert the directed flow of the ions to ion thermal energy. *Banks and Kockarts* [1973] give an approximate relationship for the ion temperature (their equation 22.12), which applies for times longer than the ion-neutral collision time,

$$T_I - T_n = m_n V_I^2 / 3k_B \tag{10}$$

in our notation, where T_I is the ion temperature, T_n is the neutral temperature, and m_n is the neutral mass. It should be remembered that V_I is implicitly the ion velocity with respect to the neutral atmosphere. This can be related to the electric fields observed at FAST altitudes, or from (5), the Poynting flux:

$$T_I = T_n + 10^{-2} S, \tag{11}$$

where temperatures are expressed in eV and S is the Poynting flux in mW m^{-2} at FAST. We have assumed $\Sigma_p = 8$ S, as inferred from the $\delta B/E$ ratio, and the neutrals are oxygen atoms.

From (11) it is clear that Poynting fluxes of the order of 100 mW m^{-2} will significantly raise the scale height of the ionosphere, by about an order of magnitude, assuming a typical neutral temperature of ~0.1 eV at 300 km. This will increase the column density of ions at altitudes where transverse ion heating is occurring. It has long been known that transverse ion heating is required to facilitate ion escape [e.g., *Klumpar et al.*, 1984]. A variety of wave modes have been invoked [*Norqvist et al.*, 1998], but we will not discuss these here. Suffice it to say that there clearly are waves in the ELF range within the cusp, as shown in Plate 2. In particular, while most of the events indicate the presence of proton gyroharmonics (e.g., orbit 8277), the spectrum is broadband for orbit 8276. The waves necessary to provide the transverse heating are present, and the field-aligned current within the cusp is a reasonable candidate free-energy source for wave growth.

5. Summary and Conclusions

Intense outflows of ions of terrestrial origin have been observed by the Polar spacecraft, in association with the passage of an interplanetary shock and CME on September 24-25, 1998 [*Moore et al.*, 1999]. By fortuitous coincidence the orbit of the FAST spacecraft was in the noon-midnight meridian, allowing the spacecraft to pass directly through the low-altitude cusp region. Markedly increased upward ion fluxes were observed in the cusp region for the spacecraft pass immediately following the sudden impulse. These ion outflows were coincident with enhanced cusp precipitation and enhanced Poynting flux into the ionosphere. However, while quantitatively different, the signatures were qualitatively similar from one cusp passage to the next.

Given the similarity in signatures, we discussed the expected effect of the magnetic flux transport at the magnetopause on the cusp-region ionosphere. In particular, on the basis of the "B, v paradigm" [*Parker*, 1996], we emphasized the dependence of cusp-region signatures on the orientation of the IMF. At the magnetopause, reconnection is expected near the cusp for all orientations of the IMF [*Crooker*, 1979], not just southward IMF. Furthermore, the y-SM magnetic field deviations at FAST altitudes clearly followed the polarity of the IMF B_y, again indicating that cusp reconnection is controlling the cusp-region currents and associated Poynting flux.

There are several features of the cusp-region observations not necessarily germane to the issue of ion outflow but clearly warranting further study. The cusp precipitation is embedded within the lower-latitude field-aligned current of the pair of cusp-region currents. A small portion of this lower-latitude current sometimes extends onto closed field lines, while the cusp precipitation is on open field lines. The less dense and generally less disturbed return current is at higher latitudes, well within the polar cap. The FAST observations are consistent with the current system sketched in Figure 4c, where the cusp currents merge into the region 1 current system. Because the FAST observations reported here were acquired during an interval of very strong IMF B_y, we put forward the speculation that the other current systems shown in Figure 4 could apply for increasingly northward IMF. These results should be investigated further with more cusp-region data.

Returning to the cause of the enhanced ion outflows, we found that there was a significant correlation between peak ion flux and peak Poynting flux for a small sample of orbits around the time of the sudden impulse. Because the interval under investigation may be unusual, given the intensity of the fluxes, analysis of more data is again warranted. Nevertheless, for the most intense outflows the peak Poynting flux into the cusp-region ionosphere was very large, ~120 mW m^{-2} at FAST altitudes. Taking into account field-line mapping, this would correspond to ~500 mW m^{-2} at the ionosphere. It is worth comparing this with the canonical electron energy flux of 1 mW m^{-2} (1 erg cm^{-2} s^{-1}) required to give 1 kR of auroral emissions. Although the complete mechanism has not been specified in detail, such a large energy flux must have consequences. Following *Banks and Kockarts* [1973], the Joule dissipation heats the ions within the ionosphere, and the resultant increase in ionospheric scale height increases the column density of ions at altitudes where transverse heating occurs. At even higher altitudes, additional acceleration may also occur, such as the centrifugal acceleration postulated by *Cladis* [1986]. Thus the electromagnetic energy flux is not the sole cause for the ion outflows, but it is the necessary first step. Within the cusp region this energy flux appears to be a direct consequence of the reconnection of cusp-region field lines.

Acknowledgments. Wind key parameter data were provided by K. W. Ogilvie and R. P. Lepping. FAST data analysis at the University of California was supported through NASA grant NAG5-3596. Additional support was provided by the NASA ISTP program under UPN 37[0]-17-43 at NASA/GSFC, grant NAG5-3171 at UCLA, and contract NAS5-30302 at Lockheed Martin. This is IGPP publication number 5434.

Hiroshi Matsumoto thanks K. Marubashi and another referee for their assistance in evaluating this paper.

References

Amm, O., M. J. Engebretson, R. A. Greenwald, H. Lühr, and T. Moretto, Direct determination of IMF B_y-related cusp region current systems, using SuperDARN radar and multiple ground magnetometer data: A link to theory on cusp current origin, *J. Geophys. Res.*, *104*, 17,187–17,198, 1999.

Banks, P. M., and G. Kockarts, *Aeronomy, Part B*, Academic, San Diego, Calif., 1973.

Bonnell, J., R. C. Elphic, S. Palfery, R. J. Strangeway, W. K. Peterson, D. Klumpar, C. W. Carlson, R. E. Ergun, and J. P. McFadden, Observations of polar cap arcs on FAST, *J. Geophys. Res.*, *104*, 12,669–12,681, 1999.

Carlson, C. W., R. F. Pfaff, and J. G. Watzin, The fast auroral snapshot (FAST) mission, *Geophys. Res. Lett.*, *25*, 2013-2016, 1998.

Cladis, J. B., Parallel acceleration and transport of ions from polar ionosphere to plasma sheet, *Geophys. Res. Lett.*, *13*, 893–896, 1986.

Cowley, S. W. H., Magnetospheric asymmetries associated with the Y-component of the IMF, *Planet. Space Sci.*, *29*, 79–96, 1981.

Crooker, N. U., Dayside merging and cusp geometry, *J. Geophys. Res.*, *84*, 951–959, 1979.

Klumpar, D., W. K. Peterson, and E. G. Shelley, Direct evidence for two-stage (bimodal) acceleration of ionospheric ions, *J. Geophys. Res.*, *89*, 10,779–10,787, 1984.

Lee, L. C., J. R. Kan, and S.-I. Akasofu, On the origin of cusp field-aligned currents, *J. Geophys.*, *57*, 217–221, 1985.

Lockwood, M., and M. F. Smith, Low and middle altitude cusp particle signatures for general magnetopause reconnection rate variations, 1, Theory, *J. Geophys. Res.*, *99*, 8531–8553, 1994.

Moore, T. E., W. K. Peterson, C. T. Russell, M. O. Chandler, M. R. Collier, H. L. Collin, P. D. Craven, R. Fitzenreiter, B. L. Giles, and C. J. Pollock, Ionospheric mass ejection in response to a coronal mass ejection, *Geophys. Res. Lett.*, *26*, 2339–2342, 1999.

Norqvist, P., M. André, and M. Tyrland, A statistical study of ion energization mechanisms in the auroral region, *J. Geophys. Res.*, *103*, 23,459–23,473, 1998.

Parker, E. N., The alternative paradigm for magnetospheric physics, *J. Geophys. Res.*, *101*, 10,587–10,625, 1996.

Pollock, C. J., T. E. Moore, D. Gurnett, J. A. Slavin, and J. H. Waite Jr., Observations of electric and magnetic field signatures in association with upwelling ion events, *Eos Trans. AGU*, *69*(44), 1396, 1988.

Russell, C. T., X. W. Zhou, P. J. Chi, H. Kawano, T. E. Moore, W. K. Peterson, J. B. Cladis, and H. J. Singer, Sudden compression of the outer magnetosphere associated with an ionospheric mass ejection, *Geophys. Res. Lett.*, *26*, 2343–2346, 1999.

Strangeway, R. J., R. C. Elphic, W. J. Peria, and C. W. Carlson, FAST observations of electromagnetic stresses applied to the polar ionosphere, in *Magnetospheric Current Systems, Geophys. Monogr. Ser.*, vol. 118, edited by S.-I. Ohtani et al., pp. 21–29, AGU, Washington D. C., 2000.

Tsyganenko, N. A., Effects of the solar wind conditions on the global magnetospheric configuration as deduced from data-based field models, in *Proceedings of the ICS-3 Conference, Versailles, France, May 12-17, 1996, Eur. Space Agency Spec. Publ., ESA SP-389*, 181–185, 1996.

Wilhjelm, J., E. Friis-Christensen, and T. A. Potemra, The relationship between ionospheric and field-aligned currents in the dayside cusp, *J. Geophys. Res.*, *83*, 5586–5594, 1978.

Zanetti, L. J., T. A. Potemra, T. Iijima, W. Baumjohann, and P. F. Bythrow, Ionospheric and Birkeland current distributions for northward interplanetary field: Inferred polar convection, *J. Geophys. Res.*, *89*, 7453–7458, 1984.

C. W. Carlson, J. P. McFadden, and M. Temerin, Space Sciences Laboratory, University of California, Berkeley, CA 94720.

R. E. Ergun, Laboratory for Atmospheric and Space Physics, University of Colorado, Boulder, CO 80303.

D. M. Klumpar and W. K. Peterson, Lockheed Martin Advanced Technology Center, Palo Alto, CA 94304.

T. E. Moore, NASA Goddard Space Flight Center, Greenbelt, MD 20771.

C. T. Russell and R. J. Strangeway, Institute of Geophysics and Planetary Physics, University of California, Los Angeles, 405 Hilgard Ave., Los Angeles, CA 90095-1567. (strange@igpp.ucla.edu)

(Received October 26, 1999; revised February 15, 2000;
accepted February 15, 2000.)